Bulgarian Chemical Communications, Volume 43, Number 2 (pp. 264–275) 2011

Potential of neutron diffraction for disclosure of structural details after chemical substitution

K. A. Krezhov*

Institute for Nuclear Research and Nuclear Energy, Bulgarian academy of sciences, 72 Tzarigradsko chaussee, 1784 Sofia, Bulgaria

Received January 7, 2011; Revised April 19, 2011

Neutron diffraction is nowadays a well established non destructive technique with proven high efficiency in solving complex structural problems in condensed matter. The technique exploits the unique properties of the neutron that make it an especially versatile probe in crystallographic research. Neutrons penetrate through many engineering materials and can be used in complex sample environments, feel hydrogen and light atoms in presence of heavy atoms in general, can detect isotope substitutions and distinguish adjacent elements in the periodic table, and are highly sensitive to magnetism. We give examples of recent applications of neutron diffraction with an emphasis on experiments in nanoscience and magnetism.

Key words: Transition metal oxides; Neutron scattering; Crystal structure; Magnetic structure.

INTRODUCTION

Among the ways the science has learned to produce new materials the chemical substitution is one of the most popular ones. Lately, multi-functional materials fell in the focus of intensive investigations because of possibility to combine multiple functions including mechanical, electronic, photonic, optical, biological, and magnetic functions, and to be capable of exhibiting diverse controllable, and predictable physical responses when subjected to various external conditions.

This paper is motivated by the recent resurgence of interest in complex oxides owing to their coupling of electrical, magnetic, thermal, mechanical, and optical properties, which make them suitable for a wide variety of applications. With many advantages over other forms of radiation, neutrons have made significant contributions towards a detailed understanding of structure-property relationships. In contrast to other probes utilized in structural investigations such as electrons and X-rays, the neutrons have the ability to reveal nuclear positions and mean displacements without bias from the effects of electron distribution.

After a brief presentation of the basic concepts of neutron scattering we will give examples of neutron diffraction and emphasis on the use of thermodiffractometry to follow magnetic phase transitions will be also commented.

THE NEUTRON

More than half of all "visible" matter in the universe is made of neutrons. Except for the neutron component of cosmic rays reaching the Earth, they are bound deep inside the atomic nucleus and it is not easy to free them out. Free neutron is a subatomic particle of mass $m_n = 1.175\times10^{-27}$ kg, which according to the quark theory, is constituted by two down (d) and one up (u) quarks giving it a neutral charge.

Within the limits of the very small uncertainty of advanced experiments the neutron has a "zero" electric charge ($q_n/e \leq (-0.4\pm1.1)10^{-21}$, e – charge of electron) and "zero" electrical dipole moment (d_n<6.3 10^{-26} *ecm*), but the internal quark structure tolerates an electric charge distribution measured as mean quadratic radius of charge. The charge distribution entails a magnetic moment $\mu_n = -1.913042\ \mu_N$ (μ_N is the nuclear magneton) and an electric polarisability α_n $\left(\alpha_n = \left(0.98^{+0.19}_{-0.23}\right)10^{-3}\,\mathrm{fm}^3\right)$, 1 fm = 10^{-13} cm.

Expressed via the Pauli matrices $\hat{\sigma}$ (spin operator $\left(\frac{1}{2}\hat{\sigma}\right)$), the neutron magnetic moment is $\hat{\mu}_n = -\gamma\mu_N\,\hat{\sigma}$, where the minus sign reflects the experimental fact that the directions of neutron magnetic moment and neutron spin are opposite, the coefficient γ = 1.91304273(45) is determined experimentally with high accuracy [1].

* To whom all correspondence should be sent:
E-mail: krezhov@inrne.bas.bg

Because the neutron bears a magnetic moment this gives the possibility with far reaching consequences: why not to make the neutron to become polarized; i.e. to probe the details of matter with well oriented in space "magnetic needles".

The free neutron is unstable in time and decays in proton, electron and antineutrino. The short neutron life time (mean time $\tau = 886.9 \pm 0.9$ s, half-time $T_{1/2} = 614.1 \pm 0.6$ s [2]) is not essential for experiments in condensed matter; neutrons of velocities of the order of 250÷5000 m/s are used so that the decrease in neutron number due to neutron β-decay at distances of the order of several meters up to some hundred meters is negligible.

The *production of neutrons* on a large scale is based on nuclear reactions (Figure 1).

The *nuclear reactor* is using a controlled nuclear fission reaction. The most common source of neutrons is the fission process of nuclei such as ^{235}U in most reactors designed for research experiments or ^{239}Pu being the case of the pulsed reactor IBR-2 of the Joint Institute for Nuclear Research (JINR) in Dubna, Russia.

In another case of using nuclear reactions, different accelerator based neutron sources were developed; neutrons are generated from the bombardment of a target with high energetic particles such as electrons, protons or deuterium. The so-called "*spallation neutron sources*" proved to combine high safety and high neutron generation efficiency.

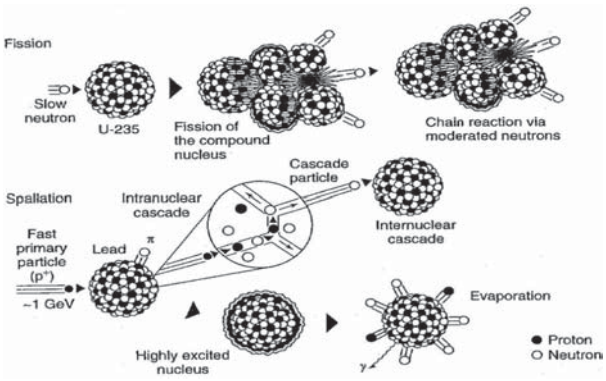

Fig. 1. Schematic drawing of neutron production by fission of 235U nucleus (upper part) and spallation on the example of a heavy target (lower part)

When a fast particle with λ shorter than the linear dimensions of the nucleus, for instance a high-energy proton ($E_p \approx 0.60 - 1$ GeV), strikes a heavy atomic nucleus (Pb, Hg, W, Ta, ^{238}U) some of its neutrons are "spalled" or knocked out from the nucleus in a nuclear reaction called *spallation.* Other neutrons are "*evaporate*d" as the bombarded nucleus heats up. In principle, the spallation is a stochastic process where particles as protons, muons, neutrinos as well as neutrons are spalled from the nucleus. Presently, the most intense neutron sources use proton accelerators. For every proton bombarding the target nucleus 15 up to 30 neutrons could be emitted depending on the target.

Because of the neutron mass the neutrons generated by fission or spallation can be slowed down (*moderated*) by collisions with light atoms such as hydrogen (H) or deuterium (D) to energies that are favourable for particular studies. The energy ranges roughly correspond to the temperature of the moderator material (Table 1). From the energy range (E<1 keV) of "slow neutrons" in nuclear physics one uses "*hot*" (E ≈ 100–500 meV; λ ≈ 0.5–1 Å) produced by heated (T > 2000 K) bloc of graphite, "*thermal*" (E ≈ 10–100 meV; λ ≈ 1–3 Å) moderated by a vessel containing water at room temperature and "*cold*" (E ≈ 0.1–10 meV; λ ≈ 3–30 Å) – by liquid hydrogen or deuterium (T< 30K).

These energy ranges are corresponding to those of lattice vibrations (phonons) or spin excitations (magnons) and thus creation or annihilation of a lattice wave produces a measurable shift in neutron energy (inelastic scattering). Also, the energies are comparable to vibrational and diffusional energies of molecular systems and are appropriate for detection of molecular motion in the frequency range of 10^7–10^{14} Hz. This dynamic range covers the slow dynamics of polymer reptation up to high frequency diatomic oscillations. The wavelengths are in the range of typical atomic distances so interference

Table 1. Classification of neutrons by energy in condensed matter research

Neutrons		Wavelength (nm), typical	Velocity (m/s)	Temperature (K)	Energy (eV)
epithermal or hot		0.07	5700	2000	0.170
thermal		0.18	2200	300	0.025
	cold	0.4	1000	58	0.005
cold	very cold	6.6	60	0.2	2×10^{-5}
	ultra cold	58.2	6.8	3×10^{-3}	2×10^{-7}

occurs between waves scattered by neighboring atoms (diffraction) [3].

Independently of the way of production, *neutron guides* are used to channel beams of the moderated to lower energies "spalled" or "fission" neutrons that probe material structure and properties to the *neutron spectrometers*. The moderated neutron beams are "white" with a Maxwellian distribution of neutron velocity and neutrons with a broad range of energies can be used for "*time-of-flight*" and "*time-resolved*" (in case of a sufficiently intense neutron flux) measurements [4] but a given wavelength can be appropriately selected for measurements with monochromatic beams.

A low energy (non-relativistic) neutron has energy E, wavelength λ and wave vector $\vec{k}$ directed along the neutron velocity $\vec{v}$. These quantities are related:

$$|\vec{k}| = 2\pi/\lambda,\ \lambda = h/(m_n|\vec{v}|),\ E = m_n v^2/2, \quad (1)$$

where h is Planck's constant and m_n is the mass of the neutron. Approximate conversions are as follows:

$$E\ [\text{meV}] \approx 81.8042/(\lambda[\text{Å}])^2 \approx 2.072\ k^2 = 5.227\ v^2 = 0.08617\ \text{T},$$

where T is temperature in units K (Kelvin) and v[mm/μs] ≈ 4/λ[Å]

The most commonly used units of neutron wavelength and energy are the Ångström (Å) and the millielectron volt (meV) respectively: 1 Å = 0.1 nm and

$$1\ \text{meV} \approx 0{,}242 \times 10^{12}\ \text{Hz} \approx 8.07\ \text{cm}^{-1} \approx 11.6\ \text{K} \approx 17.3\ \text{Tesla} \approx 1.6\times10^{-15}\ \text{erg}.$$

Hence, 1 kJ/mol ≈ 10.4 meV/molecule.

Owing to lack of charge to cause ionization in a medium, the neutrons cannot be directly detected. Thermal neutrons are usually detected by sensing the nuclear reaction products following neutron capture. BF_3 gas counters employ the reaction $^{10}B_5 + {}^1n_0 \rightarrow {}^7Li_3 + {}^4He_2 + 2.7$ MeV, the helium-3 gas counters use $^3He_2 + {}^1n_0 \rightarrow {}^3He_1 + {}^1H_1 + 0.77$ MeV and film/scintillators: $^6Li_3 + {}^1n_0 \rightarrow {}^3H_1 + {}^4He_2 + 4.79$ MeV. Fission chambers with ^{235}U are most often used to monitor the neutron beam stability in time.

SCATTERING, REFRACTION AND ABSORPTION: CROSS-SECTION FORMALISM

Figure 2 schematically outlines the outcomes when a beam of neutrons hits a material. The fraction of neutrons propagating along a new direction is named "scattered" neutrons, and the investigation of materials by measuring how they scatter neutrons is known as *neutron scattering.*

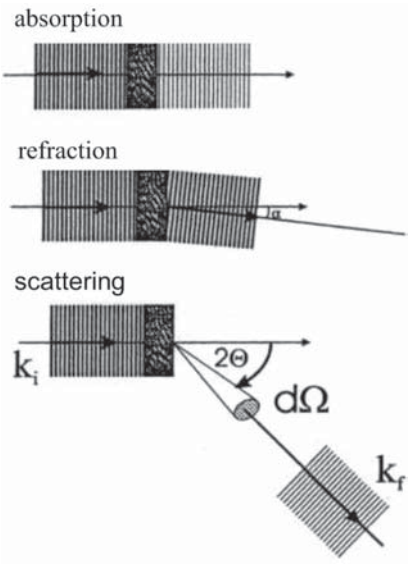

Fig. 2. The three cases of interaction of a monochromatic neutron beam with matter when propagating through a given medium $|\vec{k}_0| = |\vec{k}_i| = 2\pi/\lambda \Rightarrow |\vec{k}| = |\vec{k}_f| = 2\pi/\lambda'$.
Absorption: the transmitted beam preserves the initial direction of propagation but its intensity is lower than incident beam intensity.
Refraction: the intensity is preserved but the direction of propagation slightly changes. The refraction coefficient $n \approx 1$ (the deviation is of the order of $\pm10^{-5}$) and the angle of deflection α is of the order of one degree)
Scattering: the beam changes both intensity and propagation direction (scattering angle 2Θ).

The registered quantity in scattering experiments is the intensity I_s of the particles (neutrons), which after interacting with the scatterers are propagating along a certain direction in space and eventually one measures the change in their energy.

The geometry of the scattering event is illustrated schematically in Figure 3.

The incident neutron with wave vector $\vec{k}_0$ (momentum $\hbar\vec{k}_0$) and energy $E_0 = (\hbar\vec{k}_0)^2/2m_n$ is registered by a detector, positioned under an angle 2θ with respect to $\vec{k}_0$, as a neutron with wave vector $\vec{k}$ and energy $E = (\hbar\vec{k})^2/2m_n$. The "wave vector transfer," or "*scattering vector,*" is. The cosine rule $\vec{Q} = \vec{k}_0 - \vec{k}$, applied to the (Q, k_0, k) scattering triangle in Figure 3, gives $Q^2 = k_0^2 + k^2 - 2k_0$ kcos (2θ), where 2θ is the "*scattering angle*" (the angle between the incident and scattered neutron beam directions). For the special case of *elastic scattering* holds $E_0 = E$, hω= 0, $k_0 = k$, and $Q = 2k_0 \sin\theta = 4\pi\sin\theta/\lambda_0$, where λ_0 is the incident wavelength.

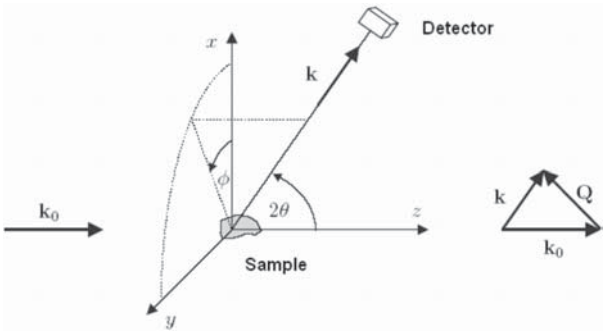

Fig. 3. Geometry of a scattering experiment. The detector collects the neutrons scattered in a solid angle $d\Omega = \sin 2\theta\, d(2\theta)d\varphi$. In elastic scattering studies the vectors $\vec{k}$ и $\vec{k}$ are of equal length $2\pi/\lambda$. The scattering vector $\vec{Q}$ is measured in reciprocal angstroms [Å^{-1}].

The physics in the scattering problem is to disclose what has happened with the momentum $\hbar\vec{Q}$ and energy ΔE transferred to the scatterers:

$$\vec{Q} = \vec{\kappa} = \vec{k}_0 - \vec{k}, \quad \Delta E = \hbar\omega = E_0 - E = \frac{\hbar^2}{2m_n}(k_0^2 - k^2). \qquad (2)$$

Expressed through the wavelength the expressions (2) have the form:

$$Q = \kappa = 2\theta \quad \frac{1}{\lambda_0^2} + \frac{1}{\lambda^2} \quad \frac{2}{\lambda_0\lambda}\cos 2\theta \quad {}^{1/2}, \quad \hbar\omega = \frac{\hbar^2}{2m} \quad \frac{1}{\lambda_0^2} \quad \frac{1}{\lambda^2} \qquad (3)$$

The "*double differential cross-section*", $(d^2\sigma/d\Omega dE)d\Omega dE$, measures the probability that the neutron is scattered within an elementary solid angle $d\Omega = \sin 2\theta d(2\theta)d\varphi$ with a transferred energy ΔE in the interval E_0, E_0+dE. The full neutron cross section is:

$$\sigma = \int d\Omega \left(\frac{d\sigma}{d\Omega}\right) = \int d\Omega \int dE \left(\frac{d^2\sigma}{d\Omega dE}\right). \qquad (4)$$

The basic assumption in using the cross-section formalism is that the probability for neutron scattering in a uniformly irradiated homogeneous sample is proportional to the sample volume. For a given substance the cross-sections are presented per effective chemical unit (formula unit), an atom of a monoatomic substance or a molecule, if the notion is applicable. Thus, the cross section σ or the differential cross-section $d\sigma/d\Omega$ is expressed through the full intensity of the scattered beam I or with the infinitesimal intensity dI under different scattering angles within the solid angle $d\Omega$: I [n/s] = $\varphi\, N\, \sigma$ and dI [n/s] = $\varphi\, N\, d\sigma/d\Omega$. Here, N is the number of formula units in the sample, and the neutron flux (number of incident neutrons per unit time on unit area perpendicular to the direction of neutron propagation) is:

$$\Phi = \Phi(E)\, \eta\, d\Omega\, dE/4\pi, \qquad (5)$$

where $\Phi(E)$ is the energy distribution of the neutron source flux in the energy interval E, E+dE and $\eta < 1$ reflects the intensity loss owing to the finite effectiveness of the scattering setup.

The theory of neutron scattering in first Born approximation gives "*the master formula*":

$$\frac{d^2\sigma}{d\Omega dE} = \frac{k}{k_0}\left(\frac{m}{2\pi\hbar^2}\right)^2 \sum_{\nu_0 s_0} p_{\nu_0} p_{s_0} \sum_{\nu s} \left|\langle ks\nu\,|\hat{V}|\,k_0 s_0 \nu_0\rangle\right|^2 \delta\left(\Delta E + E_\nu - E_{\nu_0}\right), \qquad (6)$$

where p_{s_0} and $p_{\nu_0} = e^{-\frac{E_{\lambda_0}}{kT}} / \sum_\nu e^{-\frac{E_\lambda}{kT}}$ are the population factor of initial states (for unpolarized beam the polarization states $p_{s_0} = \frac{1}{2}$ for $s_0 = \pm\frac{1}{2}$. It describes that a neutron wave with wave vector $\vec{k}_0$ and spin s_0, after interacting with matter is registered at a distance r with wave vector $\vec{k}$ and spin s. The quantum state of the target (scatterers) changes from $|\nu_0\rangle$ to $|\nu\rangle$, accompanied with change in energy state from E_{ν_0} to E_ν. In (6) ν stands for the set of quantum number describing spin and orbital electronic states, phonons, isotope distribution, orientation of nuclear spins etc in the target.

The interaction potential $\hat{V}$ is a sum of two components. The first one is arising from the strong neutron-nucleus interaction. It causes "*nuclear scattering*" and can be described by the so-called Fermi's pseudo potential depicted schematically in Figure 4:

$$\hat{V}(\vec{r}) = \sum_i \frac{2\pi\hbar^2}{m} b_i \delta\left(\vec{r} - \vec{R}\right), \qquad (7)$$

Where δ is the Dirac delta function and the quantity b is the asymptotic scattering amplitude: $\lim_{\kappa\to 0}|f(\vec{\kappa})| = -b$. In principle, it is a complex quantity: b = b′ – ib″. The real part b′ is positive for most

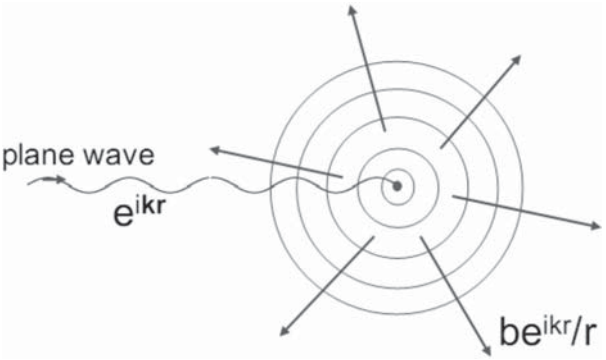

Fig. 4. Nuclear scattering described by the pseudopotential of Fermi: The neutron represented by a plane wave is scattered on the nucleus, which is a point-like object, as spherical waves. The amplitude of the spherical wave is governed by a parameter b known as the scattering length.

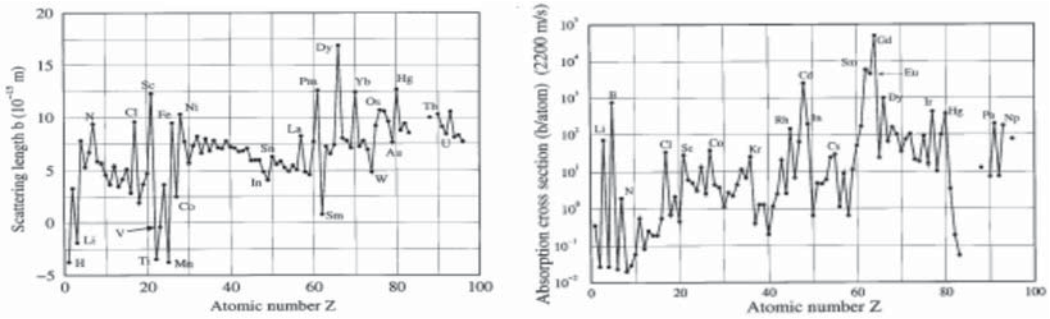

Fig. 5. Left) The real part of the neutron scattering length b; Right) the absorption cross-section for velocity of neutrons 2200 m/s

elements and is in the range 0.3 $10^{-12} \div 1.1\ 10^{-12}$ cm. For ^{1}H (proton), ^{7}Li, ^{48}Ti, ^{51}V, ^{55}Mn, ^{62}Ni, ^{152}Sm and some others it is negative (Fig. 5, Left panel). For most nuclides the imaginary part $b'' = (k/4\pi)\sigma_a(k)$, which gives rise to the absorption of neutrons, is very small. Here $\sigma_a(k)$ is the absorption cross-section, which is a quantity that covers roughly six orders of magnitude. The values $\sigma_{abs} = \sigma_a(k)$ also vary, occasionally significantly, from one isotope to another. For example σ_{abs} = 940 b/atom for ^{6}Li but only 0.045 b/atom for ^{7}Li.

For a given nucleus b is a fundamental constant; it has dimension of length (10^{-12} cm) and is known as the *Fermi scattering length*. The values of b are accurately measured and tabulated for all elements and nearly all their isotopes [5]. The isotopic differences allow the use of *isotope substitution* and *contrast variation*, which permits highlighting of parts or whole molecules to distinguish them in complex or multicomponent systems. Widely used is the deuterium labelling because $b_D = +6.67\ 10^{-12}$ cm, $b_H = -3.74\ 10^{-12}$ cm.

In early days of neutron scattering the microscopic cross section σ was evaluated from the macroscopic cross section Σ measured from neutron transmission experiments with pure chemical substances (Fig. 6).

The mean potential $\langle \hat{V}(\vec{r}) \rangle$ has the periodicity of the crystal lattice and can be expanded in Fourier series in the reciprocal space.

$$\langle \hat{V}(\vec{r}) \rangle = \frac{1}{N\vartheta_0} \sum_{\vec{\tau}} \exp(-i\vec{\tau}\vec{r}) V_{\vec{\tau}} \qquad (8)$$

where $\vartheta_0 = \vec{a}(\vec{b} \times \vec{c})$ and N are correspondingly the volume of the unit cell and the number of unit cells in the volume of the crystal, and the Fourier components are determined by:

$$V_{\vec{\tau}} = \int d\vec{r} \exp(i\vec{\tau}\vec{r}) \langle \hat{V}(\vec{r}) \rangle = N \frac{2\pi\hbar^2}{m} F(\vec{\tau}), \qquad (9)$$

where $\vec{\tau} = h\vec{a}^* + k\vec{b}^* + l\vec{c}^* = \vec{\tau}_{hkl}$ is the reciprocal lattice vector. In (9) it is introduced the quantity $F(\vec{\tau})$ – structure factor of the unit cell:

$$F(\vec{\tau}) = \frac{m}{2\pi\hbar^2} \int_{\vartheta_0} d\vec{\tau} \exp(i\vec{\tau}\vec{r}) \langle \hat{V}(\vec{r}) \rangle. \qquad (10)$$

By substituting (10) in (6), for the general form of the differential cross section of coherent elastic scattering of thermal neutrons by a potential with the period of the crystal lattice we get:

$$\left(\frac{d\sigma}{d\Omega}\right) coh = \frac{\gamma e^2}{m_e c^2} \frac{(2\pi)^3}{\vartheta_0} N \sum_{\vec{\tau}} \delta(\vec{\kappa} - \vec{\tau}) |F(\vec{\tau})|^2 \qquad (11)$$

The expression (11) is general; it does not depend on the interaction potential and is valid for both nuclear and magnetic interaction. One should have in mind that generally the crystalline and the magnetic lattices do not have the same periodicity. The delta-function tells us that the scattering occurs only for $\vec{Q} = \vec{k}_i - \vec{\kappa}_f = \vec{\tau}$. Going back to the real space one easily derives the familiar form of Bragg's law: $n\lambda = 2d\sin\theta$.

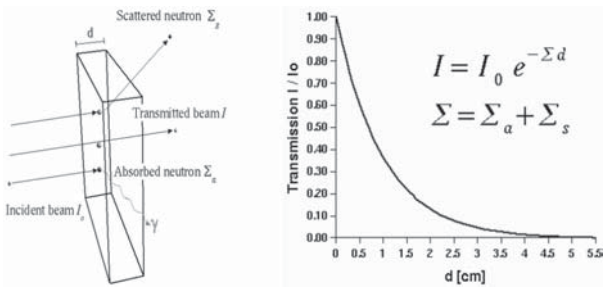

Fig. 6. The attenuation of a narrow neutron monochromatic beam passing a material layer of thickness d [cm] obeys exponential law: Σ – total macroscopic cross section [cm^{-1}], σ – total microscopic cross section, ρ – density [gcm^{-3}], A –atomic weight [$gmol^{-1}$], $\Sigma = N\sigma$ [cm^{-1}], the number of nuclei per unit volume $N = (\rho/A)N_A$, [cm^{-3}], N_A – Avogadro number

MAGNETIC SCATTERING

In (6) the second component in $\hat{V}$ causes "*magnetic scattering*" and arises from the interaction of neutron with the magnetic induction **B** = **M** + **H** within the sample. Generally, **B** is connected with presence in the sample of atoms that have electron shells with unpaired electrons. The potential of magnetic interaction between the neutron magnetic moment operator $\hat{\mu}_n = -\gamma\mu_N\hat{\sigma}$ and the magnetic field $\vec{H}$, created in point $\vec{R}$ by an electron with a magnetic moment $\hat{\mu}_e = -2\mu_B\hat{s}$ moving with velocity $\vec{V}_e = \hat{p}_e/m_e$ is [6]:

$$\hat{V}_\mu(\vec{R}) = -\frac{\gamma\hbar_e}{mc}\hat{\sigma}\vec{H} = -\frac{\gamma\hbar_e}{mc}\hat{\sigma}\left\{rot\left[\frac{\hat{\mu}_e\times\vec{R}}{|\vec{R}|^3} + \frac{(-e)}{c}\frac{\vec{V}_e\times\vec{R}}{|\vec{R}|^3}\right]\right\}. \quad (12)$$

The first term in (12) arises from the spin of the electron and the second term comes from its orbital motion.

The evaluation of the transition matrix elements in (6) has been carried out for the scattering of both unpolarized and of polarized neutron beams for many classes of magnetic media: paramagnets, ferromagnets, antiferromagnets. The Fourier transform of the atomic magnetization density at the site of every magnetic ion is called *magnetic form factor*. The calculations are rather complicated.

In a magnetically ordered state of the compounds, the computations of magnetic scattering have revealed presence of different kinds of long-range magnetic order, collinear and noncollinear arrangements of spins (atomic magnetic moments) as well as a number of hellical spin structures (magnetic spiral structures). Figure 7 illustrates the geometry of magnetic scattering. For unpolarized neutrons the magnetic cross section has the form [7]:

$$\left(\frac{d\sigma}{d\Omega}\right)coh = \frac{\gamma e^2}{m_e c^2}\frac{(2\pi)^3}{\vartheta_0}N\sum_{\vec{\tau}}\delta(\vec{\kappa}-\vec{\tau})\left|\vec{e}\times(\vec{F}(\vec{\tau})\times\vec{e})\right|^2. \quad (13)$$

The constant p = $r_e\gamma/2$ = 0.2695 allows converting the Fourier components of atomic magnetic moments in magnetic scattering amplitudes given in units 10^{-12} cm. The magnetic scattering amplitudes and nuclear scattering lengths are of the same order of magnitude. In favourable cases one can introduce the quantity "magnetic unit-cell structure factor", which is a vector

$$\vec{F}_M(\vec{\tau}) = \sum_{\vec{\tau}} f_\tau(\vec{\tau})\mu_\tau\exp(i\vec{\tau}.\vec{R}_t), \quad (14)$$

where the sum runs over all magnetic atoms, $f_\tau(\vec{\tau})$ is the magnetic form-factor of the atom with localized moment μ_τ and the elastic magnetic scattering cross-section from an ordered magnetic structure is proportional to $\sum_{\vec{\tau}}\delta(\vec{\kappa}-\vec{\tau}_M)\left|\vec{F}_{M\perp}(\vec{\tau})\right|^2$ with $\vec{F}_{M\perp}(\vec{\tau}) = \vec{\tau}\times\vec{F}_M\times\vec{\tau}$.

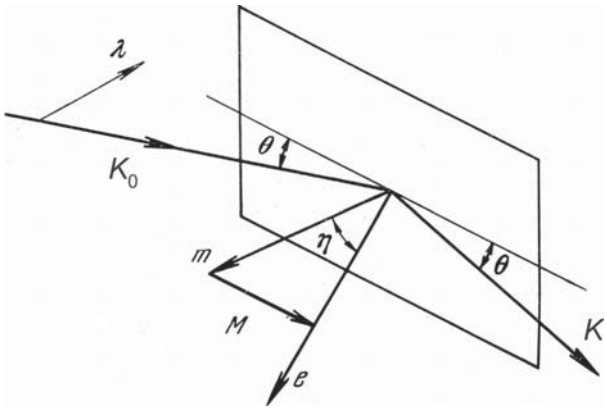

Fig. 7. Schematic drawing of the magnetic scattering of neurons [7] from a medium with magnetization $\vec{M}$ and relation between vector $\vec{q} = \vec{M}$, unit vector $\vec{e}$ and unit vector $\vec{m}$ (in direction of an atomic magnetic moment). Vector $\vec{q} = \vec{M}$ lies always in the scattering plane. For a beam of polarized neutrons the direction of the vector of neutron polarization $\vec{\lambda}$ is also important for the scattering cross-section

If the magnetic and nuclear unit cells do not coincide, then magnetic Bragg scattering is observed at different reciprocal lattice vectors $\vec{\tau}_M$. In paramagnetic state these magnetic peaks are not present and this could be a further advantage for the structure determination.

DISORDER

The interaction potential $\hat{V}(\vec{r})$ between neutron and crystal, strictly speaking, does not possess the crystal lattice periodicity. The reasons are of two kinds: *statistical deviations* due to isotope disorder, magnetic impurities, orientation of nuclear spins and *dynamic deviation*s due to atomic and electronic motion [8]. Even so, the crystal as a whole has a periodic structure. It can be defined that the neutron "sees" a mean potential $\left\langle\hat{V}(\vec{r})\right\rangle = \sum_{v_0} p_{v_0}\langle v_0|\,\hat{V}(\vec{r})\,|v_0\rangle$, the local deviation from which is $\delta\hat{V}(\vec{r})$ such that $\sum_{v_0} p_{v_0}\langle v_0|\hat{V}(\vec{r})\,|v\rangle = 0$:

$$\hat{V}(r) = \left\langle\hat{V}(\vec{r})\right\rangle + \delta\,\hat{V}(\vec{r}). \quad (15)$$

Substitution of (15) in (6) gives:

$$\frac{d^2\sigma}{d\Omega\,dE} = \left(\frac{d^2\sigma}{d\Omega\,dE}\right)_{incoh} + \left(\frac{d^2\sigma}{d\Omega\,dE}\right)_{coh} \quad (16)$$

The first term in (16) reflects the mechanisms that lead to incoherent scattering and depends weakly on the scattering angle via the Debye-Waller factor $\exp(-W_{\vec{d}}(\vec{\tau}))$ describing thermal vibration of atoms

about their mean positions. The second term in (16) contributes to the interference Bragg scattering. Beyond the so-called Bragg "cutoff wavelength" λ_c, which is such that the Bragg equation $\lambda_i = 2d_{hkl} \sin\theta$ cannot be satisfied for $\lambda_i > \lambda_c$, there is no coherent scattering whatsoever (neglecting atomic disorder).

THE PAIR CORRELATION CONCEPT

This concept was worked out by van Hove in 1950-ies with the aim to describe the distribution of momentum and energy transfers in a scattering process in terms of the correlation between scattering centres in space and time. It is valid for the case of slow neutron scattering by liquids, gases, and crystals when the Born approximation holds. As it was shown by Van Hove (6) could be expressed in the form [9]:

$$\frac{d^2\sigma}{d\Omega dE} = \frac{k_f}{k_0} N \frac{\sigma_t}{4\pi} S(\vec{Q},\omega), \qquad (17)$$

where $\sigma_t \equiv 4\pi\left\langle \overline{b^2} \right\rangle = 4\pi N^{-1} \sum \overline{b_i^2}$ is the mean full neutron cross-section and the function $S(\vec{Q},\omega)$, known as "scattering function" or else "scattering law", is given by:

$$S(\vec{Q},\omega) = \frac{2}{2\pi\hbar N\left\langle \overline{b^2} \right\rangle} \int_{-\infty}^{\infty} dt e^{-i\omega t} \sum_{k,l} \overline{b_k b_l} \langle e^{-i\vec{Q}\cdot\vec{r}_k(t)} e^{i\vec{Q}\cdot\vec{r}_l(t)} \rangle. \qquad (18)$$

The $S(\vec{Q},\omega)$ scattering function has dimension of reciprocal energy [E^{-1}] and does not contain variables related with the wave functions of the incident and scattered neutrons, expressed in other words, it does not depend on the velocities **v** and $\mathbf{v_0}$. The only valid quantities are the momentum transfer $\vec{Q} = \vec{k}_0 - \vec{k}_f$ and the energy transfer $\Delta E \equiv \hbar\omega = E_0 - E_f$, i.e. the combination of only 4 parameters. From the point of view of theory the way of realizing the acts of transfer is not of importance. Therefore, equation (6) and correspondingly (9) specify that the probe and the target system are decoupled. This is a very important characteristic of neutron scattering; the neutrons being a very weakly interacting probe just monitor an unperturbed state of the target. Often $S(\vec{Q},\omega)$ is called dynamic structure factor.

Hence, in the scattering experiment one measures the summary intensity, where beside interference maxima there is always present incoherent background. The difference between the coherent and incoherent scattering is important because it gives different information for the system. Incoherent scattering gives information for the single particle correlation function, which determines the probability to find a particle at the point with radius vector $\vec{r}$ at time t, if the same particle was located at point $\vec{r}$ =0 at time t=0. The coherent scattering gives information for the pair correlation function, i.e. the probability to find an atom at origin at $\vec{r}$ =0 at time t=0 and another atom at $\vec{r}$ at time t. The coherent scattering probes the general properties of a large assembly of atoms: the spatial order or the lattice dynamics. Incoherent scattering allows studying the behaviour of a single scatterer (atom), such as the diffusion of given atomic species in the crystal lattice.

The main uses of beams of neutrons in condensed matter research are summarised in Figure 8 and Table 2. Eight cross sections are matter of importance.

The standard method of analyzing the neutron powder diffraction patterns, known as *Rietveld method* or else *full profile refinement*, is to fit the parameters of a model of the crystal and magnetic structure to the measured profile, which is the scattered neutron intensity measured as a function of scattering angle 2θ. The Rietveld method is a structure refinement method, not a structure solution method. It must always be remembered that although neutron diffraction is an extremely powerful technique, it should be used in conjunction with other techniques to fully exploit its potential.

Figure 9 illustrates structure refinement for nanocrystalline goethite [10] with average particle size $D \approx 10\times80$ nm as determined from scanning electron microscopy images.

The figure illustrates the extensive incoherent scattering of hydrogen from the hydroxyl group of goethite most probably enhanced additionally by crystalline water, i.e. actually FeO(OH).nH(OH). This is reflected by the steadily rising contribution to instrumental background with decreasing to zero scattering angles. We found our nanomaterial to preserve orthorhombic Pnma symmetry of microc-

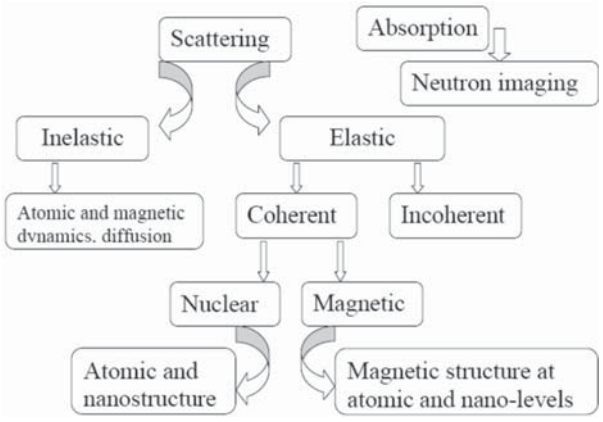

Fig. 8. Interaction of low energy neutrons and condensed matter fields of investigations

Table 2. The neutron as a probe in condensed matter research

1. No electric charge. Weak interaction characterized by a small cross section and hence high penetration capability	The scattering can be treated on the basis of the first Born approximation Voluminous samples can be investigated Specialized environment is easily used: thick-walled sample cans, high pressure chambers, high and low temperature furnaces
2. Scattering on nucleus known as "nuclear scattering"	One can distinguish: elements, isotopes, e.g. "hydrogen from deuterium" ⇒ the contrast variation method
3. Magnetic moment. Scattering on the magnetic field generated by the unpaired electrons of atomic shells	The magnetic properties can be investigated on microscopic level and to analyze the magnetic structure ⇒ antiferromagnetism, spiral spin order and other arrangements
4. The wavelength of thermal neutrons is comparable with inter-atomic distances	One can determine both the crystalline structure (symmetry, atomic positions) and the magnetic structure (magnetic symmetry, location, mutual orientation and magnitude of magnetic moments)
5. The thermal neutron kinetic energy falls in the range of elementary excitations	The dynamic properties and excitation energies can be investigated
6. Coherent and incoherent scattering processes can be distinguished	Both collective phenomena and single atom effects (for instance diffusion) can be studied

rystalline material and to order in antiferromagnetic spin arrangement with coinciding crystalline and magnetic unit cells with parameters a=4.6049(9) Å, b=9.958(3), c = 3.022(1) Å. The magnetic structure we determined as canted antiferromagnetic with a slightly reduced effective magnetic moment of cation Fe^{3+}: 2.78(12) μ_B instead 2.98(4) μ_B known for the bulk material.

Nanomaterials are receiving increasing attention in the technical and scientific communities. The reason that size matters is that the properties of materials can have some unexpected differences from their behaviour in larger bulk forms that opens up new application opportunities. Two reasons for this change in behaviour are the increased relative surface area (producing increased chemical reactivity) and the increasing dominance of quantum effects with impact on the material's optical, magnetic, or electrical properties.

Figure 10 represents the thermal evolution of the NPD pattern of $La_{0.5}Pb_{0.5}FeO_3$ material with average particle size $D = 80 \pm 15$ nm obtained by combustion route [11].

The appearance of additional diffraction lines of magnetic origin below $T_N = 558 \pm 5$ K is in good correspondence with the phase transition at T = 554.2 ± 0.2 K analyzed by DTA/TG measurements. Symmetry analysis gave the magnetic mode

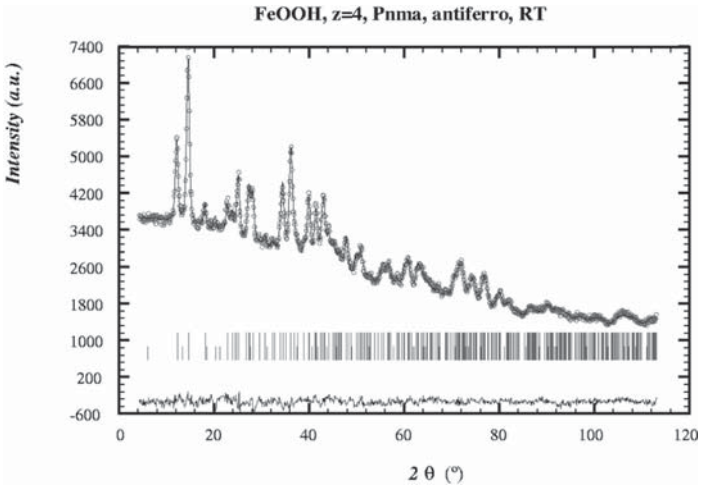

Fig. 9. Rietveld refinement (continuous line) of neutron diffraction data (circles) measured at room temperature on powder material of nanocrystalline FeO(OH). The neutron wavelength is 1.0571 Å. The difference curve between experiment and calculation is shown at the bottom. The background curve is smoothly approximated by a polynomial of 5-th order.

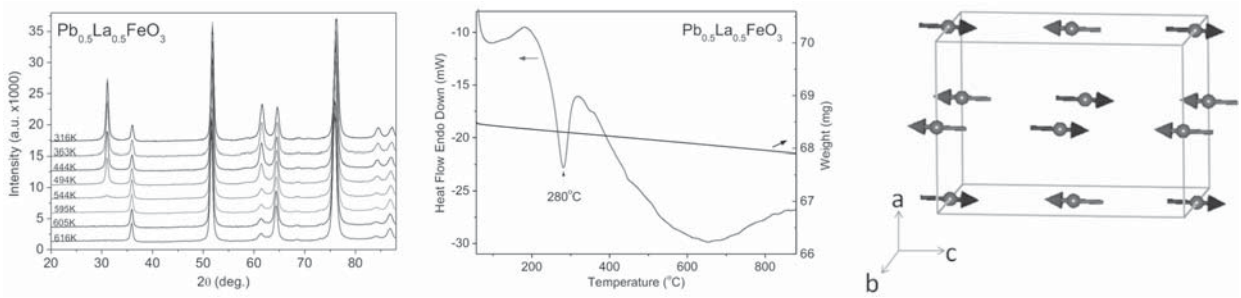

Fig. 10. a) Thermal evolution of neutron scattering upon heating; b) DTA/TGA: no mass loss → evidence for magnetic transition, c) G-type magnetic structure.

Γ_4 (G_x, A_y, F_z; f_z) with $f_z = 0$ (La is non-magnetic), $A_y \approx 0$, $F_z \approx 0$, and $S_x \approx (3.6 \pm 0.2)\ \mu_B$.

Today to attain better understanding of the magnetism and the magnetic behaviour of systems with reduced dimensions is of utmost importance. Figure11 illustrates on the example of substituted barium hexaferrites [12] that neutron diffraction allows seeing details in both the magnetic and the atomic ordering that were affected due to grain size reduction and cation substitution. Concerning microwave applications as absorbing media, the substitution by non-magnetic Sc ions is known to reduce substantially the ferrimagnetic resonance frequency of $BaFe_{12}O_{19}$. On the other hand, substitution of Fe^{3+} by the Co^{2+}/Ti^{4+} pair is among the most often used ways to enhance magneto-optic effects in the range of wavelengths appropriate for recording technologies.

There is a reasonable understanding of the physics of simple systems without competing magnetic interactions. Many systems, however, exhibit competing interactions, that is, interactions that do not all favour the same magnetic ordered state. In this case not all interactions can be minimised simultaneously, best example is the antiferromagnetic exchange interactions on a triangular lattice, and the system is said to be magnetically frustrated [13]. Also, cases when ordered magnetic moments systematically involve 3d or 4f unpaired electrons lead to unexpected results. Sufficiently strong competition (a high degree of frustration) leads to new physics that is manifested by the appearance of noncolinear ordering, novel critical exponents, rich phase diagrams, or an absence of long-range magnetic order at low temperatures, leading to magnetic analogues of liquids and ice.

Magnetism and ferroelectricity form the backbone of many fields of science and technology. Multiferroics have become an object of growing interest due to the coexistence of magnetic order (FM or AFM) and ferroelectric polarization in a single-phase material. Beside important implications for

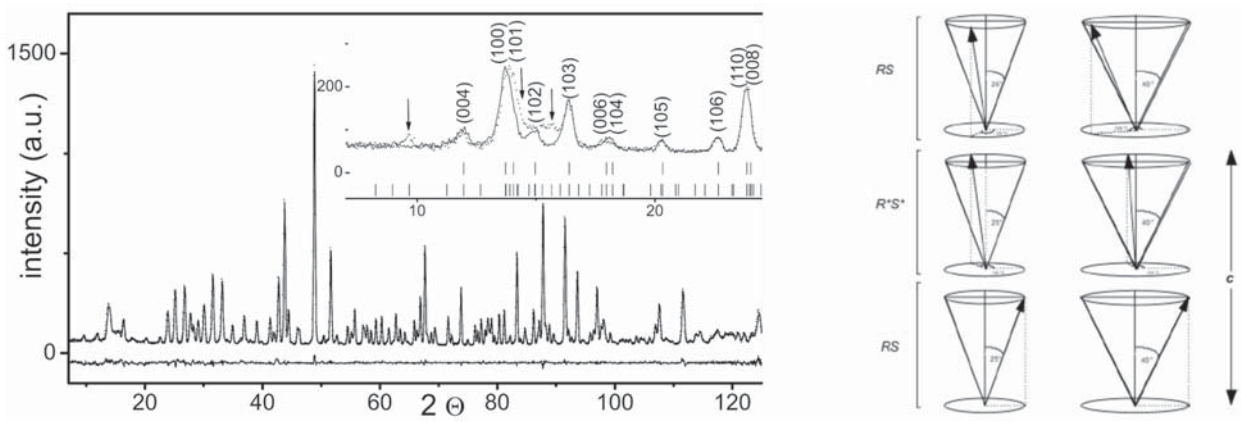

Fig. 11. a) Neutron diffraction pattern (l=1.2251 Å) of $BaFe_{10.4}Sc_{1.6}O_{19}$ at 10K and its Rietveld-refinement in the conical block-type magnetic structure in space group P63/mmc (a=5.9240 Å c=23.5395 Å). The inset shows the low angle part both at 10K (dots) and 300K (solid line), the arrows indicate the extra magnetic reflections at 10K; b) Block-conical magnetic structure. The phase of spin rotation is dependent on substitution; for $BaFe_{12-2x}Co_xF_{ex}O_{19}$ – phase 120° (x=0.8) and 104° (x=1.1). Incommensurate magnetic structure with cone angle ≈ 40o and propagation vector k ≈ 0.24 was found for $BaFe_{10.4}Sc_{1.6}O_{19}$.

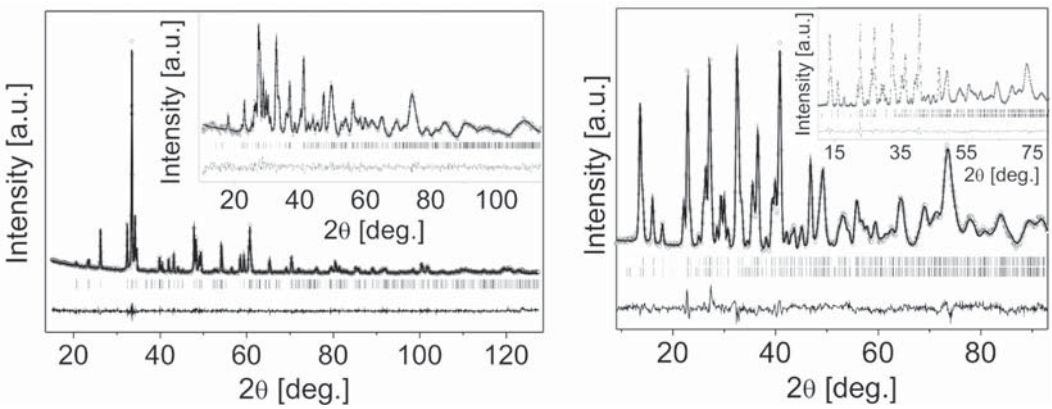

Fig. 12. NPD Rietveld plots of $YFe_{0.875}Cr_{0.125}O_3$ and $YFeO_3$ (inset) b) Simultaneous multipattern XRD and NPD (inset) refinement of $YCrO_3$ in paramagnetic weak ferroelectric state, T = 295 K

novel electronic devices such as electric-field controlled spintronic devices, electric and magnetic field sensors, electric power generators and new four-state logic memory, the physics behind the expected complex magnetoelectric phenomena is among the hot topics in condensed matter [13–16].

We investigated the solid solubility between $YFeO_3$ and $CrFeO_3$ known as weak antiferromagnets and the spin arrangements in the system YCr_{1-x}–Fe_xO_3 synthesized by combustion route [14]. The magnetic order occurs below a concentration dependent Néel temperature T_N between 648 K (x=1) and 141 K (x=0). In view of the weak biferroicity of $YCrO_3$ with transition at T_E =400 K to weak ferroelectric state much above the magnetic phase transition to weak AFM state, the evidence helps in improving our understanding of perovskite-like systems with noncollinear spin ordering. Figure 12 shows the Rietveld-refined diffraction patterns of some members of this solid solution system, demonstrating single phases with centrosymmetric average crystal structure of orthorhombic Pnma symmetry. The XRD structural data alone did not allow accurate determination of TO_6 (T=Fe,Cr) distortions and we carried out a multipattern (X ray + neutron) profile analyses. The compounds with x≥0.60 displayed AFM ordering of type G_yF_x at 295 K and with growing Fe content the weak ferromagnetic component F was found increased.

In the restricted class of multiferroic materials the mixed valence oxides with general formula RMn_2O_5 (R = rare earth metal, Y or Bi) crystallizing in perovskite-like structure are well known for the relatively strong correlations between magnetic order and ferroelectricity. Perovskites represent one of the most important classes of functional materials and also play a leading role in multiferroic research.

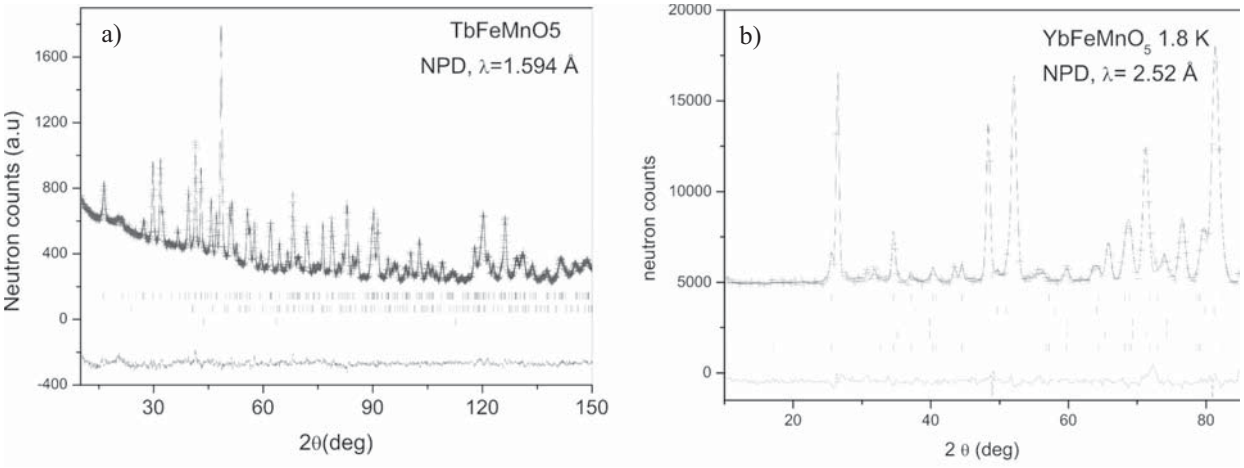

Fig. 13. a) Comparison of the observed (circles), calculated (solid line) and difference (at the bottom) NPD patterns for $TbFeMnO_5$ at T = 295 K. The second series of tick marks correspond to $TbFeO_3$ and the third series to vanadium; **b**) Rietveld plot for $YbFeMnO_5$ at T=1.8 K

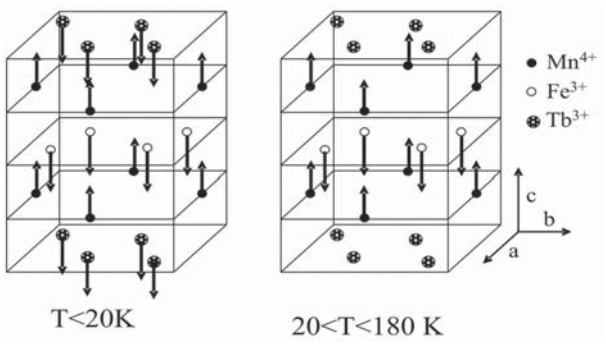

Fig. 14. Magnetic structures in $TbFeMnO_5$. The magnetic cell coincides with the chemical cell (**k** = 0)

The substitution effects we illustrate with the derivative compounds $YbFeMnO_5$ and $TbFeMnO_5$ where half of manganese is replaced by iron [15,16]. The samples were prepared in polycrystalline form by a soft chemistry route followed by thermal treatments under high-oxygen pressure. The Rietveld analysis of diffraction data showed that the crystal structure is orthorhombic, *Pbam* (SG), formed by chains of edge-linked $Mn^{4+}O_6$ octahedra linked together by dimer groups of square pyramids $Fe^{3+}O_5$ and units $R^{3+}O_8$ (R= Yb^{3+}, Tb^{3+}, respectively) (Figure 13).

The thermal evolution of the NPD patterns evidenced that below a transition temperature of $T_c \approx 160$ K for $YbFeMnO_5$ and $T_c \approx 175$ K it is developed a long-range magnetic order resolved as a ferrimagnetic arrangement of Fe^{3+} ions (4*h* site) and Mn^{4+} ions (4*f* site) spins with propagation vector **k**=0. At lower temperatures, the magnetic moment of the Yb^{3+} (Tb^{3+}) cation also participates in the magnetic structure (see Figure 14), adopting a parallel arrangement with the Mn^{4+} spins; at T = 1.8 K the magnitudes of the magnetic moments of the effective scatterers are 2.00(8), –3.04(17) and 0.35(14) μ_B, over the sites 4*f*, 4*h* and 4*g* sites respectively for $YbFeMnO_5$ whereas in the case of $TbFeMnO_5$ we evaluated $1.5(3)\mu_B$ for the Mn^{4+} cations, $-2.0(1)\mu_B$ for the Fe^{3+} cations and $3.9(2)\mu_B$ for the Tb^{3+} cations.

The relatively weak magnetic moments with respect to the expected values may be related to the antisite disordering in both sublattices, promoting AFM interactions that partially hinder the FM coupling in the chains of MnO_6 octahedra and in the Fe_2O_{10} dimmers. The lack of evidence for a crystallographic phase transition to a polar space group ruled out the expectations of a spontaneous electric polarization. In addition, the observed collinear ferrimagnetic structure with k = 0 does not allow spin polarization and the magnetic symmetry group excludes a linear magnetoelectric effect.

CONCLUSIONS

As has been discussed above, neutron scattering is a powerful and versatile tool in many research fields and with the advances in neutron sources and equipment many previously dreamed experiments such as *in situ* and time-resolved experiments, even in adverse environment, have been done nowadays. It is believed that the few examples presented will motivate the readers to speculate on the many capabilities of the neutron scattering techniques and to realize how the neutron diffraction in particular could be useful for their own investigations.

Acknowledgements: *This work is supported by the National Science Fund of Bulgaria, Project DO-02/2008.*

REFERENCES

1. http:/www.neutron.anl.gov.
2. http:/www.codata.org/ The Committee for Data in Science and Technology, 2006CODATA.
3. G. E. Bacon, Neutron Diffraction, 3-rd Edition, Clarendon Press, Oxford, 1975.
4. C.G. Windsor, Pulsed neutron scattering, Taylor and Francis, London, 1981.
5. V. F. Sears, Neutron Optics, Oxford University Press, New York, 1989.
6. S.W. Lovesey, Theory of Neutron Scattering from Condensed Matter, Vol. 1 and 2, Oxford University Press, Oxford, 1987.
7. Y.A. Izyumov, R. P. Ozerov, Magnetic neutron diffraction, Plenum Press, New York, 1970.
8. G L. Squires, Introduction to the Theory of Thermal Neutron Scattering, Dover Publications, Inc, Mineola, New York, 1996.
9. L. van Hove, *Physical Review*, **95**, 249 (1954).
10. K. Krezhov, in: 5th Congress of Balkan Geophysical Society, Belgrade, Serbia, 10–16 May, 2009, 4 pages, EAGE article 122, http://www.earthdoc.org/detail.php?pubid=21100.
11. K. Krezhov, S. Kovachev, D. Kovacheva, E. Svab, G. Andre, F. Porcher, in: AIP Conference Proceedings, 2009, vol. 1203, p. 205.
12. K. Krezhov, *Solid State Phenomena*, **159**, 175 (2010).
13. R. Ramesh, N. Spaldin, *Nature Materials*, **6**, 21 (2007).
14. S. Kovachev, D. Kovacheva, S. Aleksovska, E. Svab, K. Krezhov, *Journal of Optoelectronics and Advanced Materials*, **11 (**10), 1549 (2009).
15. M. J. Martínez-Lope, M. Retuerto, J. A. Alonso, M. García-Hernández, K. Krezhov, I. Spirov, T. Ruskov, M. T. Fernández-Díaz, *Solid State Communications*, **149** (13–14), 540 (2009).
16. M. Retuerto, M. J. Martínez-Lope, A. Muñoz, T. Ruskov, I. Spirov, K. Krezhov, M. T. Fernández-Díaz, M. García-Hernández, J. A. Alonso, *Solid State Communications*, **150** (37–38), 1831 (2010).

ВЪЗМОЖНОСТИ НА НЕУТРОННАТА ДИФРАКЦИЯ ЗА УТОЧНЯВАНЕ НА СТРУКТУРНИ ДЕТАЙЛИ ПРИ ХИМИЧНО ЗАМЕСТВАНЕ

К. Крежов*

Институт за ядрени изследвания и ядрена енергетика, Българска академия на науките, бул. „Цариградско шосе“ № 72, 1784 София, България

Постъпила на 7 януари, 2011 г.; приета на 19 април, 2011 г.

(Резюме)

Между начините, по които науката се е научила да произвежда нови материали, химичното заместване е сред най-популярните. В последно време, многофункционалните материали станаха в центъра на интензивни изследвания поради възможността да се съчетават няколко функции, включително механични, електронни, фотонни, оптични, биологични и магнитни функции, както и да са способни да проявяват различни контролируеми и предсказуеми физични отговори, когато са подложени на различни външни условия. Тази статия е мотивирана от възраждането напоследък на интереса към сложни оксиди поради взаимодействието на електрическите, магнитните, топлинните, механичните и оптични свойства, което ги прави подходящи за широк спектър от приложения. От времето на пионерските експерименти на Шал и Уолан преди повече от 50 години, неутронната дифракция се прилага за справяне със сложни структурни проблеми във физиката и химията на твърдото тяло. Методиката се възползва от уникалните свойства на неутрона, които го правят особено подходяща сонда в кристалографските изследвания. Неутроните са чувствителни към водород и леки атоми в общия случай и са силно чувствителни към магнетизма. За разлика от други сонди, използвани в структурните изследвания като електрони и рентгеново лъчение, неутроните са в състояние да разкрият положенията на ядрата и средните отмествания без да се повлияват от ефектите на електронното разпределение. Ние илюстрираме тази област с изследвания на ефектите от химично заместване в различни материали. Примерите включват семейството на перовскитите и експерименти, насочени към подобряване на разбирането на някои от основните аспекти на механизмите допринасящи към вътрешно присъщи ефекти, като например подреждането на орбитали и заряди и мултифероизма, които са израз на силно взаимодействие между степените на свобода по орбитала, заряд и спин в тези системи. Структурните заключения се съчетават с резултатите от магнитни и електрически измервания и Мьосбауерова спектроскопия.